DESIGN AND NUMERICAL SIMULATION OF A NOVEL ELECTRICAL MACHINE FOR WIND ENERGY GENERATION

Safa AFFI [1], Jamel BELHADJ [2], Habib CHERIF [3, *]

This research contributes to the understanding and application of the hybrid excited flux-switching machine in small-scale wind turbine power generation. The authors conducted an extensive investigation employing a 2D finite element model to match the machine with wind turbine specifications and to comprehensively investigate the machine's design parameters and geometric sizing. The research focused on determining the appropriate physical dimensions and configuration factors, considering material properties and operational requirements to ensure structural integrity and reliability. NSGA-II algorithm is used to optimize the active part of the machine, resulting in an optimized design outcome. The study underlined the role of magnetic bridge and coil parameters in low-speed operation, with the 24/20 generator standing out for its effective regulation of key parameters enabled by dual excitation.

Keywords: renewable energy systems; flux switching machine; hybrid excitation; wind turbine design; low variable-speed; finite element

1. Introduction

Nowadays, the increasing demand for enhanced energy security and environmental awareness has spurred the drive for electric machinery to become more streamlined and effective. Consequently, as an alternative to conventional energy sources, many developed nations are enhancing energy security by harnessing renewable resources, leveraging technological and financial support to cultivate local sustainable energy sources and domestic power generation [1,2]. To seamlessly integrate cost-effective sustainable energy systems like wind turbines and photovoltaic panels, a multi-faceted optimization approach can be employed to refine system architecture and component design [3]. On another side, small wind turbines designed to operate on residential, commercial, or small industrial buildings are an important tool to achieve local scale energy production. They also

[1] PhD, Université de Tunis, ENSIT, Tunis, Tunisia and Université de Tunis El Manar, Laboratoire des Systèmes Electriques, Tunis, Tunisia, e-mail : affi.safaa@gmail.com
[2] Prof., Université de Tunis, ENSIT, Tunis, Tunisia and Université de Tunis El Manar, Laboratoire des Systèmes Electriques, Tunis, Tunisia, e-mail : jamel.belhadj@ensit.rnu.tn
[3]* Prof., Université de Tunis, ENSIT, Tunis, Tunisia and Université de Tunis El Manar, Laboratoire des Systèmes Electriques, Tunis, Tunisia, corresponding author, e-mail : habib.cherif@ensit.rnu.tn

play a potential role in satisfying the field of rural electrification and in decentralizing of energy to meet the consumers' needs [4].

According to the literature, flux-switching generators could be a prominent candidate for such applications. It can be categorized into 3 families based on their different excitation modes: Permanent Magnet flux-switching generators PMFSG (only PMs), Wound Fields flux-switching generators WF-FSG (only wound–fields), and Hybrid Excited flux-switching generators HE–FSMs (both PMs and wound–fields). For the PMFSG, a lot of studies have been dedicated to this category of machines in the field of wind generation power. To begin, the first PMFS wind generator was introduced by Javier and al. in [5]; a detailed design and parametric optimization of the machine as well as a comparative study between prototypes with different magnet materials to extract the energy potential of each configuration, conducted to that direct-drive flux switching generators can be possibly the best solutions for small wind turbines. The structure of an outer-rotor PMFSG with three phases is presented in [6]. The machine with 20 teeth on the rotor and three teeth on each tip of the stator has three auxiliary poles to enable the magnetic flux to flow smoothly. The paper shows that the PMFSG has a large power output at low wind speed and has a low cogging torque compared to surface permanent magnet synchronous generator (SPMSG) in the application of cross-flow type windmill. An optimal design of stator interior permanent magnet (SIPM) machine with special slot stator configuration that minimizes cogging torque for wind power applications is introduced in [7]. The machine configuration is based on the flux switching principle. This study emphasizes the importance of slots' geometric parameters to minimize the cogging torque.

Design optimization of PMFSG, 24 stator teeth /22 rotor teeth for direct-drive wind turbines, is developed in [8]. The optimization criterion is to decrease the losses in the generator, the required converter power, and the mass of the magnets. A double stator inner rotor axial air-gap flux switching permanent magnet prototype machine (AFSPM) was investigated in [9]. This design of the machine is a three-phase generator with 12 stator slots /10 rotor teeth and a nominal speed of 375 rpm intended for direct drive of small wind energy turbines. The study showed that a reluctant network model with a certain level of complexity can compete with the finite element model in terms of accuracy and computation times. It also conducts a comparative study in terms of harmonic content that the open-circuit performance of the AFSPM provides. Benjamin and al. presented in [10] a new topology of Hybrid Excited Flux-Switching Machine (HE-FSM) with active stator dedicated to high and variable speed applications. The advantage of air-gap field control is highlighted through this topology and prototypes of two combinations of stator/rotor pole -12/10 and 12/14- were built. To establish a comparative study of PM-FSM and HE-FSM, an analysis of the influence of hybridization-coefficient must be provided. It was mentioned through experience that the 14-teeth rotor

machine has a higher flux weakening operation than the 10-teeth rotor machine. The thermal behavior of the prototype machine is developed through experiments and the influence of the hybridization on the normalized output power is presented. In [11], the authors emphasize the finite element method and the magnetic equivalent circuit model of a parallel hybrid synchronous machine devoted to a car application. The decisive factors of the chosen method for the machine modeling are CPU time calculation and the accuracy of the results.

The novelty of the presented work arises from the fact that there is a dearth of self-consumption small wind energy initiatives in Tunisia. This situation underscores the distinctive context in which this work is applicable. In particular, the evolution of markets for small-scale wind turbines has underscored the need for inventive wind generator designs. In this work, the authors focus on the wind energy conversion system on the design of its generator, and they propose, for the first time, a Hybrid-Excited Flux-Switching (HE-FS) generator design applied to the wind power generation at small scale rotational speeds. For this, a HE-FS generator (24/20) designed specifically for a direct drive wind application (without gearbox) with a typical operating range for low-power wind sites was studied. Hybrid-Excited Flux-Switching generators offer several key advantages, making them particularly well-suited for wind energy applications. These machines are characterized by a high number of pole pairs, which naturally align with the low rotational speeds typical of wind turbines. Their rotor is entirely passive, composed of laminated magnetic sheets. This design enhances mechanical robustness and eliminates the risks of overheating associated with permanent magnets in conventional machines, as well as wear-related issues found in wound-rotor systems with brushes. All magnetic sources — permanent magnets, field excitation coils, and armature windings — are housed in the stator. This structural choice provides two main benefits: first, the absence of moving parts for these components facilitates efficient cooling due to their proximity to the heat dissipation system; second, it enables accurate thermal monitoring, significantly reducing the risk of failure or severe incidents such as fire. Finally, the main advantage of double excitation lies in its magnetic flux regulation capability, achieved through simple adjustment of the excitation current. This provides valuable control flexibility, allowing for optimal operation under varying conditions.

The paper offers significant advancements including an advanced geometric and electromagnetic design of a 24/20 HE-FS generator, followed by the development of a theoretical and numerical method for power calculation using MATLAB and Ansys Electronics. Additionally, design optimization, aiming to reduce the quantity of permanent magnets while maximizing the output power, thereby enhancing the economic viability of the generator for small-scale wind energy applications.

2. Design and modeling of HE-FSM for wind energy applications

The design of a hybrid excited flux switching generator for the low-power generation must satisfy different constraints and requirements. The following characteristics, on which the design of this machine is based, are shown in previous works [10-13] that among a whole range of electric machines, the HE-FSM seems to satisfy most requirements due to its variable adjustable flux which allows a DC generation on a diode bridge. Also, the excitation coils installed in the stator part of the machine are a major asset for this machine. Besides, the use of permanent magnets installed in the stator part is the main benefit for this HEFSM in terms of creating flux at zero excitation current added to the advantage of the increasing energy efficiency.

In the context of small wind turbines, it is important also that the generator be designed and implemented considering technical and economic factors:

- Simplicity and Efficiency at low-variable rotational speeds.
- Cost minimization to meet the local market requirements.

The HEFSM is described by the numbers of stator teeth (Ns) and rotor teeth (Nr). For a low-speed generator, the number of rotor teeth must be important to achieve a desirable electrical frequency in the same range of 50Hz to ease the grid connection. In fact, the rated rotational speed N is given by

$$N=\frac{60\times f_S}{p} \tag{1}$$

where f_s is the stator electrical frequency and p is the number of pairs of poles of the rotor.

The choice of the three-phase machine structure presented in this work must respect some rules [14] which are given by a compromise between the couple N_s and N_r.

2.1. HE-FSM principle

The wind turbine system presents a notably more dependable and cost-efficient system, particularly suitable for applications in rural electrification and the extensive integration into urban sites for electricity consumption or its conversion into other energy forms. In this paper, the turbine will be linked to the hybrid-excited flux-switching generator, as depicted in Fig. 1, and connected to a DC bus via a diode rectifier. Therefore, the main criteria of the proposed chain are the supply of the required power over a variable and low range of rotation speeds, the operation without the need for a gearbox in the case of small wind turbines and the power (voltage) control through the double excitation. Note that the dual power supply is self-excited through the DC bus.

The HEFSM shown in Fig. 2 illustrates that the stator consists of 24 elementary cells, each containing an armature coil, a permanent magnet (PM), and a slot for the

excitation winding. Each of the three phases consists of eight coils connected in the series. The number of rotor teeth is 20.

The attainment of low-power generation at minimal speeds constitutes a pivotal factor in the technical requirements of the selected machine. The geometric parameters and the magnetic circuit parameters of the studied hybrid excited machine in this paper are investigated according to the application for which the synchronous machine will be designed (wind turbine systems). The selected candidate is the topology that provides the required power to generate ($P_{electromagnetic} \geq 3$kW) starting from the smallest speed wind range.

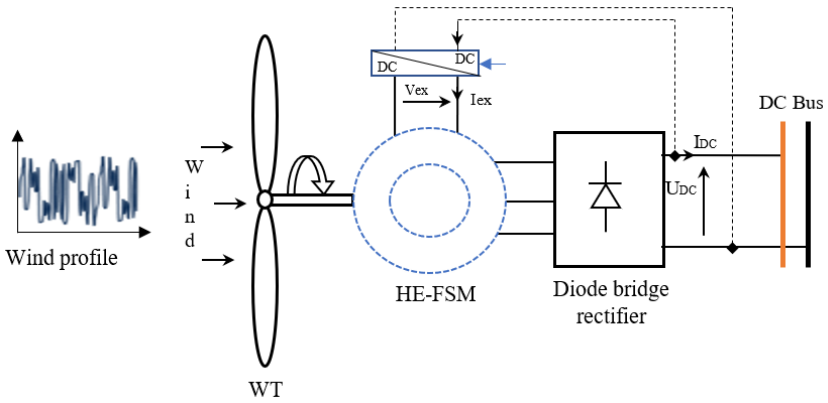

Fig. 1. The proposed wind turbine system configuration

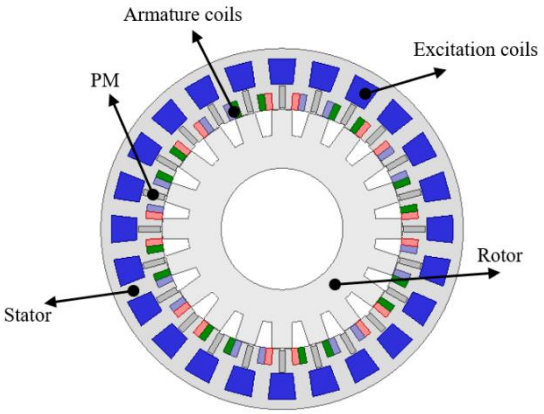

Fig. 2. Internal structure of the HEFSM highlighting the active parts of the stator

2.2. Electromagnetic output power

To calculate the generated output power, three tests must be investigated: 1) The no-load test, 2) the short-circuit current test and 3) the machine coupled to the diode bridge rectifier. The latter two tests are achieved under the electric circuit

modeling of the machine coupled to its finite element transient model. Through the proposed method, the output power could be deducted just through the second test for the zero-resistance phase. In fact, the proposed method for calculating electromagnetic power is based on the Behn-Eschenburg model. Fig.1 shows the DC alternator configuration in which the flux switching machine is associated with a diode bridge rectifier supplying a DC bus [13]. *V* and *I* are respectively the voltage and phase current in the machine with I_{DC} is the rectified current. Eq. (2) characterizes the electromagnetic output power measured via the diode bridge. The Behn-Eschenburg phase diagram (with the assumption of low value of phase resistance) conducts to the eq. (2) and the expression of the phase current *I* is derived from the square root of eq. (3).

$$P_{electro} = 3 \cdot V \cdot I \tag{2}$$

$$E^2 = V^2 + L^2\left(I_{ex}\right) \cdot w^2 \cdot I^2 \tag{3}$$

$$I^2 = \frac{1}{L^2\left(I_{ex}\right) \cdot w^2} \cdot \left(E^2\left(I_{ex}\right) - V^2\right) \tag{4}$$

$$I_{cc}\left(I_{ex}\right) = \frac{E\left(I_{ex}\right)}{L\left(I_{ex}\right) \cdot w} \tag{5}$$

Thus, the output power formulation is presented as follows:

$$P_{electro}\left(I_{ex}\right) = 3 \cdot V \cdot I_{cc}\left(I_{ex}\right) \cdot \sqrt{1 - \left(\frac{2U_{DC}}{\pi \phi_m\left(I_{ex}\right) \cdot w}\right)^2} \tag{6}$$

with I_{cc} is the short current circuit and $\phi_m\left(I_{ex}\right)$ is the maximum of no-load flux for I_{ex}.

$$P_{electro}\left(I_{ex}\right) = 3 \cdot V \cdot I_{cc} \cdot \sqrt{1 - \left(\frac{N_b\left(I_{ex}\right)}{N}\right)^2} \tag{7}$$

with, N_b (rpm) is the basic speed at which the alternator starts generating power.

$$N_b = \frac{60}{\pi^2} \cdot U_{DC} \cdot \frac{1}{N_r} \cdot \frac{1}{\phi_m\left(I_{ex}\right)} \tag{8}$$

The out-put power generation is calculated by

$$E^2 = \left(V + RI\right)^2 + \left(LWI\right)^2 \tag{9}$$

$$E^2 = V^2 + 2VRI + R^2I^2 + \left(LW\right)^2 I^2 \tag{10}$$

$$\left(R^2 + \left(LW\right)^2\right)I^2 + 2VRI + \left(V^2 - E^2\right) = 0 \tag{11}$$

$$I = \frac{1}{2\left(R^2 + L^2W^2\right)} \cdot \left(\sqrt{\left(2VR\right)^2 - 4\left(R^2 + L^2W^2\right)\left(V^2 - E^2\right)} - 2VR\right) \tag{12}$$

$$P = \frac{3U_{DC}}{\sqrt{2}\pi\left(R^2 + L^2W^2\right)} \cdot \left(\sqrt{\left(2VR\right)^2 - 4\left(R^2 + L^2W^2\right)\left(V^2 - E^2\right)} - 2VR\right) \tag{13}$$

2.3. Structural and geometric configuration of the HE-FSM

The purpose of this step is to find a set of parameters ensuring the performance specified by the requirements and criteria of the application and to find a set of parameters ensuring the optimization of the performances required by the specifications. The parametric configuration of the machine's geometry presented in Fig.3, makes it possible to investigate different topologies in terms of the number of poles. The angles and the dimensions of the rotor and the stator connect to each other via normalized parameters leading to the construction of the entire machine. The highly saturated behavior of the machines as well as the addition of several constraints and the strengthening of safety requirements in the specifications have forced designers to change their dimensioning methods and adopt a more global approach [15]. The authors present an architectural conceptual approach processing the design of the presented machine. The equations (eq.14.-eq.25) in the present section define the angular and radial parameterization of the normalized variables that delimit the geometrical sections of the machine as it is illustrated in Table 1. The shaft size is dictated by the parameter R_{shaft}, the depth of the rotor pole L_{DR} is the difference between the external radius of the rotor $R_{Ext_{Rot}}$ and its interior radius $R_{Int_{Rot}}$. The air gap radius $R_{air_{gap}}$ (eq.14) is equidistant from $R_{Ext_{Rot}}$ and the interior radius of the stator $R_{Int_{Stator}}$. This latter dimension is a function of the air gap machine thickness e (eq.15). As example, in the eq.16 $K_{R_{Bdex}}$ presents the parameter of the auxiliary excitation coil radius $R_{B_{dex}}$, $K_{H_{Bdex}}$ (eq.17) defines the parameter for the longitudinal enlargement of the coil in the stator slot $H_{B_{dex}}$ and $K_{L_{Bdex}}$ defines the

parameter for the transversal enlargement of the coil $L_{B_{dex}}$. The difference between $R_{Ext_{Stator}}$ and $R_{B_{dex}}$ defines the thickness of the magnetic bridge Δ_{mb}. The length of the permanent magnet H_{PM} is a function of the longitudinal enlargement of the excitation coil (eq.18). The radial distance bounded by the permanent magnet radius R_{PM} (eq.19) and the field coil radius (eq.20) $R_{field_{coil}}$ is equal to the ortho-radial distance bounded by the dimensioning of ϕ_{angle} . The number of the poles is one of the main determinants of the HE-FSM performances where N_r is the number of rotor slots (N_r = 20) and N_s is the number of stator slots (N_s = 24).

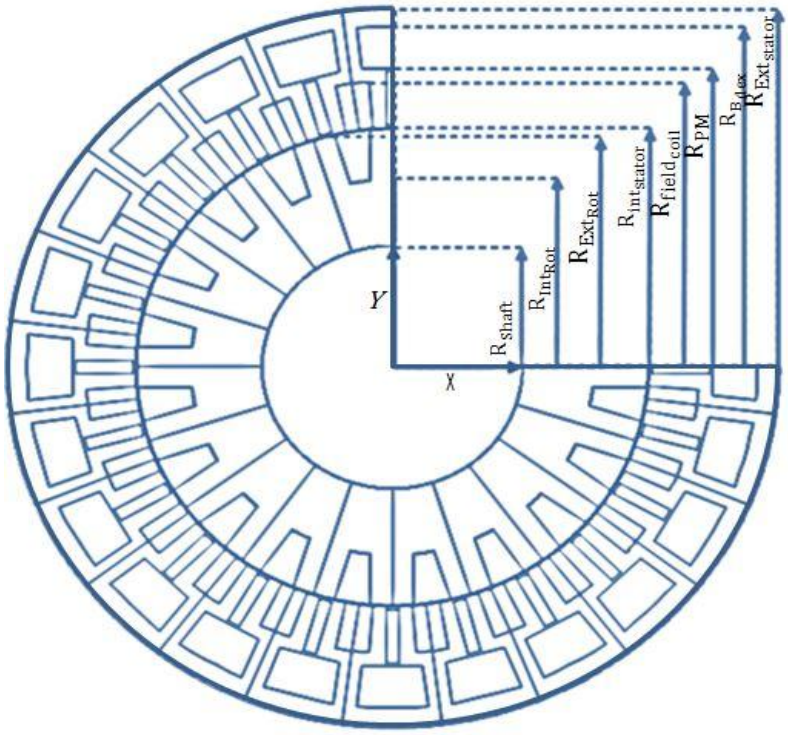

Fig. 3. The radial geometrical parameters of the HEFSM

Table 1. The sizing equations of the 24/20 HE-FS machine

Parameter	Equation		Measure
$R_{air_{gap}}$ (mm)	$k_{air_{gap}} \times R_{Ext_{stator}}$	(14)	78.1
$R_{Int_{Stator}}$ (mm)	$R_{air_{gap}} + (e \times 0.5)$	(15)	78.3
$R_{B_{dex}}$ (mm)	$K_{R_{Bdex}} \times (R_{Ext_{Stator}} - R_{Int_{Stator}}) + R_{Int_{Stator}}$	(16)	117.8
$H_{B_{dex}}$ (mm)	$K_{H_{Bdex}} \times (R_{B_{dex}} - R_{Int_{Stator}}) + 1mm$	(17)	16.78

H_{PM} (mm)	$R_{B_{dex}} - H_{B_{dex}} - 1mm$	(18)	19.27
R_{PM} (mm)	$H_{PM} + R_{Int_{Stator}}$	(19)	97.57
$R_{field_{coil}}$ (mm)	$k_{field_{coil}} \times \left(H_{PM} - R_{Int_{Stator}}\right) + R_{Int_{Stator}}$	(20)	91.5
θ_s (°)	$\frac{360}{N_s}$	(21)	15
$R_{Ext_{Rot}}$ (mm)	$R_{air_{gap}} - e \times 0.5$	(22)	77.9
$R_{Int_{Rot}}$ (mm)	$K_{Int_{Rot}} \times R_{Ext_{Rot}}$	(23)	46.3
L_{DR} (mm)	$K_{L_{DR}} \times R_{Int_{Rot}} \times \sin\left(\theta_r\right)$	(24)	13
θ_r (°)	$\frac{360}{N_r}$	(25)	18

Where R_{shaft} : the radius of the shaft, $R_{field_{coil}}$: the radius of the field coil, ϕ_{angle} : the angle between the PM and the field coil, $R_{B_{dex}}$: the outer radius of the auxiliary excitation coil, $H_{B_{dex}}$: the height of the excitation coil, $L_{B_{dex}}$: the width of the excitation coil, L_{DR} : the depth of the rotor pole, $R_{Int_{stator}}$: the inner radius of the stator, $R_{Ext_{stator}}$: the outer radius of the stator (125 mm), $R_{Int_{Rot}}$: the internal radius of rotor, $R_{Ext_{Rot}}$: the external radius of the rotor, $R_{air_{gap}}$: the radius of the air gap, H_{PM} : the length of the permanent magnet, θ_s : the angular width of the stator and θ_r : the angular width of the rotor pole.

3. Performance-based-finite element analysis of HE-FSM

To simulate the electromagnetic performances of the HE-FSM, a geometric configuration is investigated under the 2D Finite Element (FE) model. This model allows simulating the transient behavior of the machine. The angles and the dimensions of the rotor and the stator are connected to each other via normalized parameters leading to the construction of the entire machine (Table1). Figs. 4 and 5 show the stator and rotor of the digital prototype of the HE-FS machine.

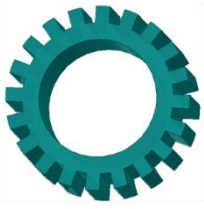

Fig. 4. The rotor configuration

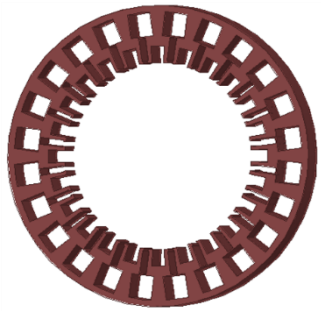

Fig. 5. The stator configuration

3.1. No-load performance evaluation of the HE-FSM

To underline the role of permanent magnets in the HE-FS machines, besides the first test of the evolution of the no-load maximum flux, a second test is investigated in which the NdFeB permanent magnets were removed from the structure and replaced by the/ air/ the SmCo permanent magnets/ the Ferrite permanent magnets. Fig. 6 presents the evolution of the no-load flux peak as a function of the excitation current per phase in the d axis for the different magnets' type. With permanent magnets, the maximum flux achieved is for a current higher than in the case without magnets ($8A/mm^2$ versus $6A/mm^2$) with a difference of $\Delta\emptyset_{max}$=0.12Wb. The SmCo and the NdFeB magnets are rare earth magnets with a higher price than the ferrite type. The NdFeB is the type of magnet that is used in this work thanks to its moderate price coupled with its high performance. However, due to the high conductivity of the (NdFeB), and slot/tooth harmonics, the eddy current loss is generated inside the magnets. This loss impacts the temperature rise inside the magnets and may lead to the unpredictable degradation of performance and potential demagnetization [16]. Excitation current regulation is obligatory to limit this demagnetization. In terms of hysteresis and saturation study, the NdFeB presents a higher level of magnetic saturation as well as higher residual magnetic flux density compared to the ferrite PMs. Beyond $8A/mm^2$ excitation current density, the flux is flexed. In fact, the flux generation of the proposed HE-FSM depends on both the rotor position and the strengthening/weakening action of the armature field to the PM field. Therefore, the flux linked in the armature windings per phase can be increased or reduced according to the operational status requests, which makes the magnetic field easily adjusted. In conventional synchronous machines, when the excitation current increases, the flux is simply limited by the magnetic saturation of the material but in no case decreases. While

dealing with the saturation problem that occurs for conventional machines, the HE-FS machines have the asset of high flux weak capability.

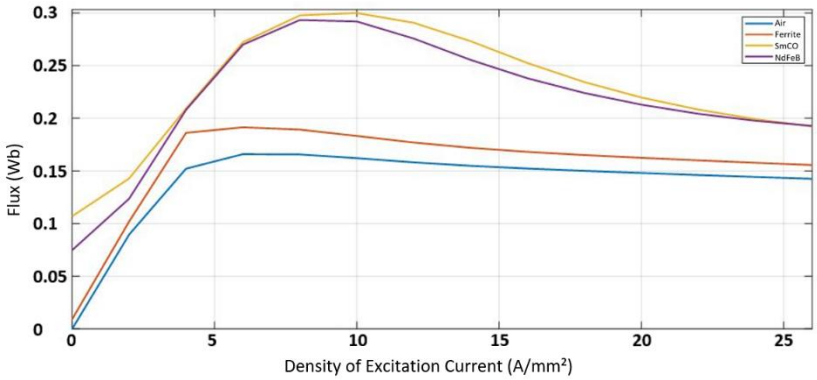

Fig. 6. No-Load flux for different magnet types

In Fig. 7, the flux density trajectories are simulated for different current excitation densities, respectively: 0 A/mm² and 4 A/mm². As seen in Fig. 7(a), under a zero-excitation current, the flux created by the permanent magnets is short-circuited in the stator through the magnetic bridge and the yoke is saturated, while only a small portion crosses the air gap, thereby forming the remanent flux. In this configuration, the magnetic bridge appears to partially neutralize the beneficial effect of the magnets. On the other hand, as soon as the excitation current is applied, it generates a magnetomotive force (MMF) that opposes the one induced by the magnets in the yoke. This phenomenon is illustrated in Fig. 7(b), where an inversion of the resulting MMF direction can be observed, causing a reversal in the flux circulation. At this stage, the stator yoke becomes less saturated, while the flux linkage through the air gap increases significantly. So, by increasing the excitation current (I_{ex} = 4A/mm^2), the saturation in the magnetic bridge is decreased and the variation of the flux is quasi-linear depending on the excitation current until reaching a maximum with an excitation current I_{ex} = 8A/mm^2.

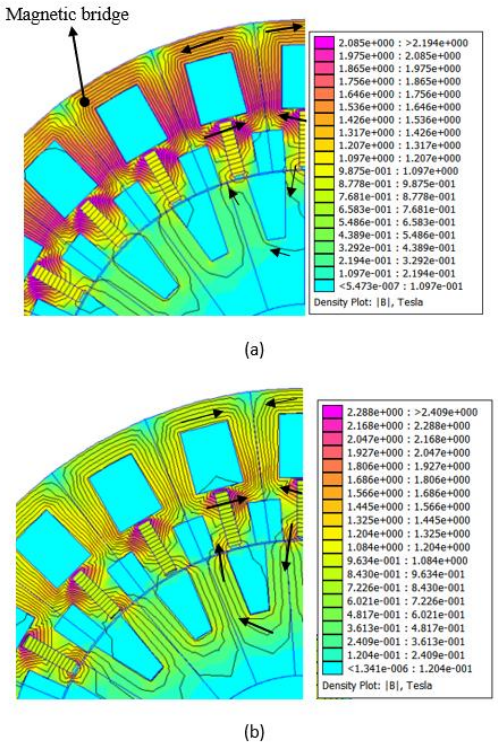

Fig. 7**.** Flux lines and no-load magnetic flux density in the HE-FSM, (a) I_{ex} = 0 A/mm², (b) I_{ex} = 4 A/mm²

The results demonstrate that, despite a low remanent voltage, the HEFSM can achieve high flux linkage. This behavior is attributed to the unique stator design incorporating a magnetic bridge, which provides enhanced control over the magnetic flux. The presence of permanent magnets in the HEFSM delays the magnetic saturation of the yoke, thereby improving the effectiveness of the excitation windings and enabling higher flux linkage levels. It is also observed that at high excitation current levels, the flux linkage decreases in both configurations. This decline is primarily due to the saturation of the stator teeth, which promotes flux leakage through the air gap.

3.2. Electric modeling of the machine under the short-circuit current test

The first method is characterized by coupling the finite element model and the electric model. In fact, it consists of coupling the transient finite element model to a circuit model. The finite element software tool (Ansys Electronics) is used to implement the equivalent armature coils in a circuit model where they will be short-circuited. From the transient model, the flux and the voltage in the coils are calculated and the information is sent to the model circuit. The evolution of the short-circuit current as a function of the excitation current density is shown in Fig.8.

In the event of a short-circuit fault during the operational mode, it is sufficient to cancel the double excitation current to avoid an increase in the short-circuit-current, thus avoiding damage to the machine. The second method of power calculation is implemented using the root-finding algorithms for each excitation current. In Fig.8, an adjustment functional area limits the excitation current density to 10 A/mm². Therefore, the current in the phase coils is also limited, the joule losses are as well-controlled and the range of the delivered power by the DC bus reaches 3kW for slow rotational speeds and under different current regulations. This adjustment functional area highlights the advantage of using the HE-FSM for such applications. The variation of the delivered power as a function of the rotational speed and excitation current density is shown in Fig.9. At zero excitation current density, a noticeable output power is delivered. Power generation starts at 400 rpm for an excitation current density of I_{exc} = 0 A/mm², whereas it starts at 300 rpm for I_{exc} = 4 A/mm². At a rotational speed of 500 rpm and without excitation current, the HE-FSM generates approximately 1 kW of power. At the same rotational speed (500 rpm), the power output of the wind turbine can be controlled through I_{exc}, allowing the machine to reach up to 3 kW.

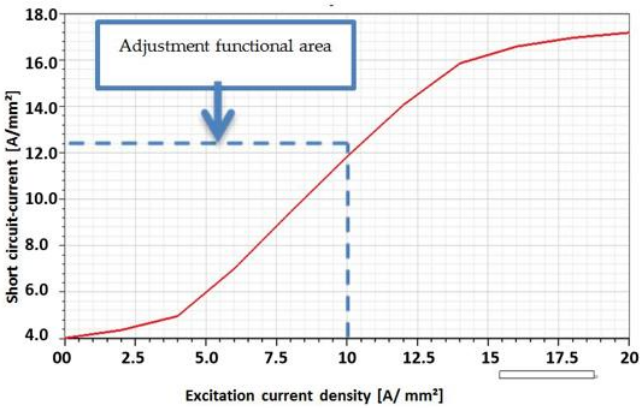

Fig. 8. The variation of short-circuit current versus the excitation current density

Ultimately, the advantageous criteria of the HE-FSM in terms of flux control and its capability of generating power from the smallest wind speeds due to the convenient hybridization of excitations, make it a reliable and interesting candidate for the presented application in this paper. Regarding the HE-FSM, the second excitation can either augment or diminish the magnetic flux based on the desired operating range [17]. Reference [11] delves into high-speed operation of the HE-FS DC-alternator, encompassing both 12/10 and 12/14 generators. In summation, in the previously presented works, the power generation scale might align with low power demands (below 10 kW); however, the operational speed range tends to be notably high and does not align with the technical characteristics of the wind power generator outlined in this study.

The 24/20 machine presented in [10, 18] has a basic speed of 1100 rpm compared to the presented machine in this paper which operates under a basic speed of 300 rpm. Thus, by comparing the performances of the prototypal machines with the proposed machine, the proposed HE-FSM has excellent characteristics in terms of output power density so it can meet efficiently the constraints studied for low variable-speed rotating machine applications.

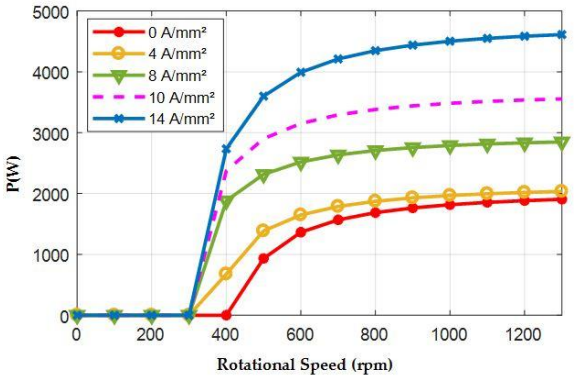

Fig. 9. Evolution of electromagnetic output power as a function of rotational speed

4. Optimization and discussion

This section investigates an optimization study on the internal geometry of the proposed machine. By using NSGA-II to optimize the active part of the studied machine, the authors have been able to find a set of solutions that present a good trade-off between different design objectives. These solutions can be evaluated and compared to the original reference machine, to determine whether they have a significant improvement. In addition, having higher number of turns per coil N_{coil} doesn't mean a higher produced power. It also could generate higher joule losses. The optimal number of turns per coil is computed by

$$N_{coil_{opt}}\left(I_{ex}\right)=\sqrt{\frac{2\times S^2}{\phi_{\max}^2\times N^2}} \tag{26}$$

with,

$$S=\frac{60\times U_{DC}}{\pi^2\times N_r} \tag{27}$$

where, $N_{coil_{opt}}$ is the optimal number of turns per coil, $\phi_{\max}$ is the maximum of no-load flux embraced per turn of the phase coil, N is the rotational speed under which the generator delivers the required power, U_{DC} is the DC bus voltage and N_r is the number of the rotor teeth.

Hereafter, in Table 2, the authors present the optimization case of study established to target the maximization of power under the lowest possible rotor speed variation. At the beginning, all the parameters of the optimization are initialized such as the number of iterations, generations and several other parameters concerning the generator operation such as the operating speeds, the voltage of the DC bus, and the initial number of turns per coil. Next, the geometrical parameters of all the particles of the generations are generated. At this stage, *C1* constraint can be evaluated (D_{pc} is the ortho-radial distance between the PM and the phase coil and $R_{B_{ind}}$ is the outer radius of the armature coil). Afterwards, the remanent flux per phase is calculated then an inverse problem is generated to define the optimal excitation current density I_{ex} with $I_{ex}= \emptyset_{max}^{-1}(I_{ex})$. Hereafter, the *Obj1* that is defined as an internal loop has been set up to find the maximum power Pmax that a structure can reach. In fact, if we go back to the expressions of the electromagnetic power, we can notice that the base speed N_b, the short-circuit current I_{cc} and the generated power depend on the number of turns per coil which must be carefully chosen. The incrimination step used here is 1 A/mm^2 with a variation interval between 0 A/mm² and 20 A/mm². This calculation is repeated until the maximum power of the investigated geometry is reached. *Obj2* and *C2* are evaluated before finding in the next step the value of the maximized power which is calculated through *Obj3*. The pareto-front of solutions is illustrated in Fig.10. The selected appropriate inner geometry for the reference machine for discussion is presented in Table 3 and Fig.11. The machine that was selected from the Pareto of solutions can efficiently generate power while simultaneously maximizing the height of the auxiliary excitation coil. This achievement is significant because it allows for the minimization of both the height and volume of the permanent magnet.

Table 2

Optimization problem formulation

Constraints	$C1: R_{B_{dex}} - H_{B_{dex}} - R_{B_{ind}} - D_{pc} = 0$ *C2*: $N_b < 400$ rpm
Objectives	*Obj1*: Inner search loop of $N_{coil_{opt}}$ *Obj2*: Minimizing the launch speed *Obj3*: Maximizing the produced electric power
Decision variables	$R_{field_{coil}}$, $H_{B_{dex}}$

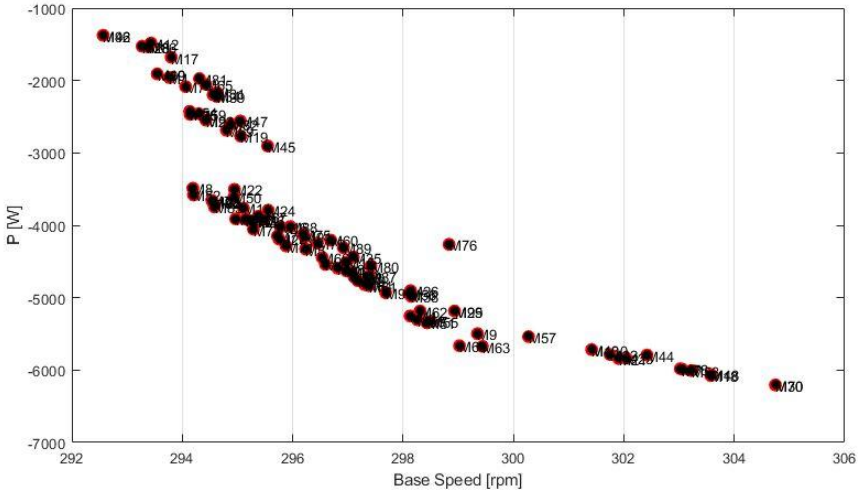

Fig. 10. Pareto-front of the solutions

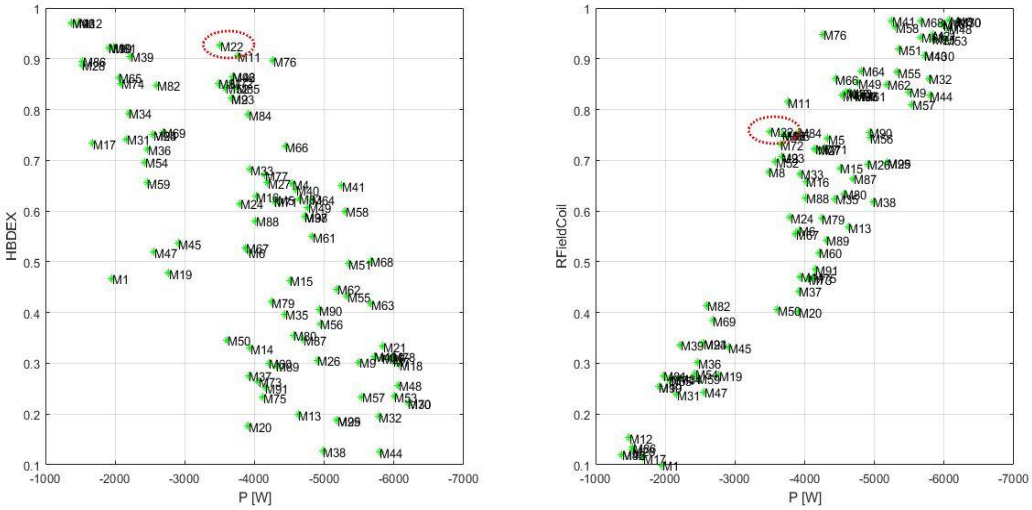

Fig. 11. The variation of the decision variables as a function of the power generated

In addition to its technical advantages, the chosen solution also holds economic benefits. One of the main cost drivers in this context is the utilization of NdFeB magnets, which can be quite expensive. However, the selected machine manages to mitigate this cost factor by minimizing the reliance on these costly magnets. As a result, the overall cost of the machine is significantly reduced, making it a financially viable option compared to the initial machine configuration. The machine's delivered power has impressively surged by 16%, underscoring its heightened power generation capabilities. Concurrently, the machine's fundamental speed has been curtailed by 3%, signifying a boost in operational efficiency.

In summary, the novel design of the proposed generator, tailored for direct drive wind applications with an emphasis on high energy efficiency and cost-effectiveness, stands poised to cater to local energy requisites. These compact wind turbines hold potential for diverse applications in both rural and urban settings. Consequently, this work presents an opportunity to recognize the demands linked to wind turbines based on wind field data and their influence on electric generator sizing.

Table 3.

Evaluation of the chosen approach in contrast to the original machine setup

Parameters	Initial configuration of the machine	Selected configuration from the Pareto of solutions	Evolution ratio of the parameters
The Height of the Auxiliary Excitation coil	16.78 mm	18.82 mm	+12%
The Height of the Permanent Magnet	19.27 mm	17.24 mm	-10%
The Height of the Field coil	12.52 mm	13.22 mm	+5.5%
The magnetic bridge thickness	8 mm	8 mm	0%
The base speed	304 rpm	294 rpm	-3.2%
The delivered power to DC bus	3000 W	3503 W	+16.7%

5. Conclusions

This paper introduces the investigation of the HE-FSM as a small wind system generator, with a focus on its performance. The system utilizes a direct-drive wind chain, optimizing cost and efficiency for low-speed, low-power wind conversion. The HE-FSM (24/20) presented here demonstrates electromagnetic power generation starting from low rotational speeds due to its high pole number and the effectiveness of excitation-hybridization in the flux switching generator. The study's findings contribute to a new generator solution for wind turbines, highlighting the importance of optimizing the hybridization between auxiliary excitation coils and permanent magnets for cost-effectiveness. The selected machine from the Pareto of solutions excels in maximizing power while controlling the height of the auxiliary excitation coil versus minimizing the height and volume of the permanent magnets. Its economic advantage lies in reducing the reliance on expensive NdFeB magnets. Additionally, the machine's performance enhancements, with a 16% increase in delivered power and a 3% decrease in basic speed, positioning it as an excellent choice as a reference machine for further in-depth topological exploration. This study highlights the potential of the direct-drive HE-FS generator as a highly efficient and viable solution for small-scale wind energy applications, particularly suited for rural areas, agricultural settings, and remote communities.

Acknowledgment

This work was supported by the Tunisian Ministry of High Education and Research under Grant LSE-LR11ES15 and PEJC 20PEJC 06-10.

R E F E R E N C E S

[1] N. Rabindra, O. M. Hammed, Energy security, renewable, non-renewable energy and economic growth in ASEAN economies: new insights, The Singapore Economic Review, Vol. 66, pp. 457-488, 2021, https://doi.org/10.1142/S0217590819430045.

[2] K. Y. Huang, G. C. Tsai, G. J. Guo, C. K. Feng, Power analysis of small wind turbine, Environmental Science and Sustainable Development, pp. 95-100, 2016, https://doi.org/10.1142/9789814723039_0013.

[3] A. Berrada, M. J. Sanjari, R. El Mrabet, Techno-economic assessment of hydrogen production: comparative analysis of electrolyser technologies in a hybrid PV/wind system, International Journal of Hydrogen Energy, Vol. 141, pp. 193-211, 2025, https://doi.org/10.1016/j.ijhydene.2025.05.384.

[4] J. Goldemberg, A. Reddy, K. Smith, R. Williams, Chapter 10: rural energy in developing countries, in *Energy and the Challenge of Sustainability*, World Energy Assessment, New York, pp. 368-389, 2015.

[5] J. Ojeda, M. Simoes, G. Li, M. Gabsi, Design of a flux-switching electrical generator for wind turbine systems, IEEE Transactions on Industry Applications, Vol. 48, pp. 1808-1816, 2012, https://doi.org/10.1109/TIA.2012.2221674.

[6] S. Kayano, M. Sanada, S. Morimoto, Power characteristics of a permanent magnet flux switching generator for a low-speed wind turbine, in Proc. International Power Electronics Conference – ECCE ASIA, Sapporo, Japan, pp. 258-263, 2010, https://doi.org/10.1109/IPEC.2010.5543884.

[7] J. Zhang, M. Cheng, Z. Chen, Optimal design of stator interior permanent magnet machine with minimized cogging torque for wind power application, Energy Conversion and Management, Vol. 49, pp. 2100-2105, 2008, https://doi.org/10.1016/j.enconman.2008.02.017.

[8] V. Dmitrievskii, V. Prakht, V. Kazakbaev, Design optimization of a permanent-magnet flux-switching generator for direct-drive wind turbines, Energies, Vol. 12, 3636, 2019, https://doi.org/10.3390/en12193636.

[9] H. Diab, Y. Amara, G. Barakat, Open circuit performance of axial air gap flux switching permanent magnet synchronous machine for wind energy conversion: modeling and experimental study, Energies, Vol. 13, 912, 2020, https://doi.org/10.3390/en13040912.

[10] B. Gaussens, E. Hoang, P. Manfe, M. Lécrivain, M. Gabsi, A hybrid excited flux-switching machine for high speed DC-alternator applications, IEEE Transactions on Industrial Electronics, Vol. 61, pp. 2976-2989, 2014, https://doi.org/10.1109/TIE.2013.2281152.

[11] S. Asfirane, S. Hlioui, Y. Amara, M. Gabsi, Study of a hybrid excitation synchronous machine: modeling and experimental validation, Mathematical and Computational Applications, Vol. 24, 34, 2019, https://doi.org/10.3390/mca24020034.

[12] A. Dupas, E. Hoang, S. Hlioui, B. Gaussens, M. Lécrivain, M. Gabsi, Performances of a hybrid excited flux switching DC-alternator: analysis and experiments, in Proc. International Conference on Electrical Machines (ICEM), Berlin, Germany, pp. 2644-2649, 2014, https://doi.org/10.1109/ICELMACH.2014.6960561.

[13] A. Nasr, S. Hlioui, M. Gabsi, M. Mairie, D. Lalevee, Design optimization of a hybrid-excited flux-switching machine for aircraft-safe DC power generation using a diode bridge rectifier,

IEEE Transactions on Industrial Electronics, Vol. 64, pp. 9896-9904, 2017, https://doi.org/10.1109/TIE.2017.2726974.

[14] Y. Amara, L. Vido, M. Gabsi, E. Hoang, H. Ben Ahmed, M. Lecrivain, Hybrid excitation synchronous machines: energy-efficient solution for vehicles propulsion, IEEE Transactions on Vehicular Technology, Vol. 58, pp. 2137-2149, 2009, https://doi.org/10.1109/TVT.2008.2009306.

[15] Z. Q. Zhu, M. M. J. Al-Ani, X. Liu, B. Lee, A mechanical flux weakening method for switched flux permanent magnet machines, IEEE Transactions on Energy Conversion, Vol. 30, pp. 806-815, 2015, https://doi.org/10.1109/TEC.2014.2380851.

[16] X. Ding, C. Mi, Modeling of eddy current loss and temperature of the magnets in permanent magnet machines, Journal of Circuits, Systems and Computers, Vol. 20, pp. 1287-1301, 2011, https://doi.org/10.1142/s021812661100789x.

[17] Y. Amara, J. Lucidarme, M. Gabsi, M. Lecrivain, A. Almed, A. Akemakou, A new topology of hybrid synchronous machine, IEEE Transactions on Industry Applications, Vol. 37, pp. 1273-1281, 2001, https://doi.org/10.1109/28.952502.

[18] M. Leimeister, A. Kolios, M. Collu, Development of a framework for wind turbine design and optimization, Modelling, Vol. 2, pp. 105-128, 2021, https://doi.org/10.3390/modelling2010006.